Multiphysics Modeling of Frontal Polymerization-Assisted Layer-by-Layer Additive Manufacturing of Thermoset Polymer Components

Zhuoting Chen[1], Morteza Ziaee[2], Mostafa Yourdkhani[2], Xiang Zhang[1*]

[1] Department of Mechanical Engineering, University of Wyoming, Laramie, WY, 82071, USA

[2] Department of Mechanical Engineering, Colorado State University, Fort Collins, CO, 80523, USA

Abstract

Frontal polymerization (FP) is a novel curing strategy that relies on a self-propagating exothermic reaction front to polymerize thermoset resins rapidly. Due to its energy-efficiency and rapid curing of thermosets, a series of applications related to polymer and polymer composite manufacturing have been developed based on FP, in particular additive manufacturing (AM). While the current research demonstrates successful printing of 1D, 2D and 3D structures based on FP, a key challenge is the determination of the printing parameters through trial-and-error, which hinders its large-scale application.

To better understand how different process parameters affect the front behavior and the printing process, and eventually enable fast printing of complex parts without trial-and-error, computational modeling of the printing process is highly desired. For the first time, we develop a multiphysics finite element model for simulating FP-assisted AM which accounts for both the thermal-chemical process and the ink deposition in a real printing process. To simulate the dynamic ink deposition process, element activation is used that constantly adds elements to the simulation domain following a predefined printing path and velocity. A coupled thermo-chemical partial differential equation system is solved over the changing ink domain to simulate the heat transfer and chemical reaction during the printing process. The model is first validated by comparing the front temperature history during the printing process with the experimental infrared

Corresponding author: xiang.zhang@uwyo.edu (Xiang Zhang)

thermal measurements. The validated model enables the determination of proper printing velocity range, within which the polymerization front can follow the printing such that the ink will not deform before curing, which is critical to ensure printing accuracy. Furthermore, the simulation reveals the change of front temperature and degree of cure between different layers, and their dependency on layer length and printing velocity, providing insights into the printing experiments for processing parameters selection.

Keywords: Multiphysics modeling; Frontal polymerization; Additive manufacturing; Thermosets; Process parameters

1. Introduction

Thermoset polymers and polymer composites have been widely used in critical engineering applications due to their excellent thermal properties, chemical resistance, and specific mechanical properties [1]. Typical manufacturing of thermosets involves molding and subsequent autoclave- or oven-based curing under elevated temperatures and vacuum conditions for an extended period of time [2,3]. Two challenges exist in this process: this manufacturing process is mostly suitable for fabricating parts with a simple geometry and is challenging to apply for manufacturing parts with complex, internal features and architectures; the traditional curing process results in high costs of manufacturing and low rates of production [4-7]. The increasingly growing demand for fabricating geometrically complex structures has accelerated research efforts focusing on additive manufacturing (AM; also known as 3D printing) of thermoset components [8-11].

AM of thermosetting polymers and composites has been previously demonstrated by direct ink writing of thermosetting ink on a *gantry* platform, followed by curing the deposited material in an oven [12]. In this approach, the ink is often cured at elevated temperature for several hours after printing, requiring a significant amount of energy

and time. Such printing process is prone to thermal yielding of ink during curing process that may lead to the loss of print fidelity [13,14]. An alternative approach for avoiding long-cycle, oven-curing process is using photocurable resin systems, where the ink is printed and immediately rigidized upon exposure to UV light to capture the prescribed geometry as the material is extruded from the nozzle. However, the existing techniques generally suffer from low cure conversion of photocurable resins during *in-situ* formation of crosslinking networks, which often results in additional post-curing steps as well as inferior mechanical properties compared with thermally curable systems [15-17].

To address this issue, a novel frontal polymerization-assisted additive manufacturing (FP-assisted AM) technique has been recently developed for rapid and energy-efficient printing of thermosets [18]. Frontal polymerization (FP) is a novel curing strategy that relies on a self-propagating exothermic reaction front to polymerize thermoset resins rapidly[19-21]. Due to its energy-efficiency and rapid curing of thermosets, FP has been used to develop a series of applications related to polymer and polymer composites manufacturing [22-27]. Another notable advantage of FP is its great compatibility with other manufacturing processes, such as ultrasound-assisted FP and concurrent polymerization and vascularization [28]. Leveraging this technique and integrating it with a 3D printing platform is another attractive application of FP, where a self-propagating reaction front can travel in tandem with the printing process, enabling supportless, energy-efficient printing of complex parts with a high degree of cure (i.e., > 95%) shortly after the ink deposition. Robertson et al. [29] presented an initial demonstration of the concept of using FP-assisted AM technique to print freeform polydicyclopentadiene (pDCPD) structures by matching the print speed with front velocity. Subsequently, Aw et al. [30] revealed a self-regulative behavior during the FP-assisted freeform AM process and used this phenomenon to print 1D, 2D, and 3D neat pDCPD structures with a high degree of cure and dimensional accuracy. Ziaee et al. [31,32] recently introduced both freeform and layer-by-layer printing of carbon fiber-reinforced composites via the FP curing of the printed ink.

While early experimental works have shown the great potential of FP-assisted AM, they rely on trial-and-error methods to determine the printing process parameters, which hinders its large-scale applications. FP-assisted AM is a multiphysics process involving cure kinetics, heat conduction, dynamic ink deposition and deformation. This leads to a large number of process parameters that could potentially affect the printing process. In the work of Aw et al. [30], a fixed 1D ink domain is chosen to study the curing behavior during printing. This model only accounts for the heat conduction along the direction of FP and the pre-calculated relationship between front velocity and ink temperature right before the reaction front. While this model revealed a self-regulative mechanism, it did not fully consider a printing process where the ink domain is continuously updated and both heat conduction and chemical reaction happen simultaneously. Without insights from modeling of a realistic printing process, existing FP-assisted printing still relies heavily on trial and error for proper selection of the printing parameters (e.g., printing speed, printing path, etc.), especially when printing a new geometry or under a different printing environment (e.g., various ambient or ink temperature). Additionally, *in-situ* analysis of cure status, internal temperature variation of filament, and front response under alternative conditions by experimental methods is quite challenging and costly. To date, modeling of a real FP-assisted AM process (i.e., 2D or 3D model with variable boundary conditions), beyond 1D simulation of the self-regulating FP curing, has not been reported in the literature to the best of the authors' knowledge. If such a model becomes available, a systematic study of the impact of the printing parameters on the printing process can be conducted to better understand and design the printing process and provide guidance to advance the applications of FP-assisted AM technique to the next level.

In this manuscript, a multiphysics model for simulating FP-assisted AM process that accounts for the coupled thermo-chemical process and dynamic ink deposition is presented for the first time. To simulate the dynamic ink deposition process, element activation is used by constantly adding elements to the simulation domain following a predefined printing path and velocity history. A coupled thermo-chemical partial

differential equation system is solved over the instantly updating ink domain to simulate the heat transfer and the chemical reaction process. The model is first validated by comparing the front temperature history during the printing process with the experimental measurements. The validated model enables the determination of proper printing velocity range, within which the polymerization front can follow the nozzle without noticeable ink deformation before curing, which is crucial for obtaining a high print accuracy. Furthermore, the simulation reveals the spatial and temporal variations of front temperature and degree of cure across different layers and their dependency on layer length and printing velocity, providing insights into the selection of the processing parameters for FP-assisted layer-by-layer printing of thermoset structures.

2. Methodology

2.1 Experimental study

2.1.1 Materials

Dicyclopentadiene (DCPD), 5-ethylidene-2-norbornene (ENB), and second-generation Grubbs' catalyst (GC2) were purchased from Sigma-Aldrich. Tributyl phosphite inhibitor (TBP, 93%) was obtained from TCI Chemicals (Tokyo, Japan). Cyclohexylbenzene (Acros Organics, 98%) was used as a solvent. All chemicals were used as received with no further purification.

2.1.2 Ink preparation

First, DCPD monomer was melted in an oven at 60 °C and mixed with 5 wt.% ENB to suppress its melting point at room temperature. This 95:5 DCPD/ENB solution is referred to as the DCPD resin hereafter. 3.852 mg GC2 (100 ppm with respect to DCPD) was dissolved in 500 μl of cyclohexylbenzene and sonicated at room temperature for 10 min. Then, 1.19 μl TBP (1 molar equivalent with respect to GC2) was added to the GC2 solution using a volumetric syringe and the resulting solution was thoroughly mixed with 6 g of DCPD. The mixture was then transferred to a 10 ml syringe and stored in an oven for 90 min at 30 °C to pre-cure the resin. Pre-curing the resin increases its viscosity and transforms it to a highly viscous gel suitable for 3D printing.

2.1.3 3D printing

The syringe barrel filled with the gel ink was placed inside an aluminum syringe holder mounted on a three-axis gantry robot (F5200N, Fisnar). The robot was equipped with a pneumatic extrusion system (DC100, Fisnar) for printing. The temperature of the ink was maintained at -5 °C using two Peltier thermoelectric cooling modules embedded inside the aluminum syringe holder to control its viscosity during the printing process. The ink was extruded through a metal nozzle with an inner diameter of 1.6 mm and printed on a hot glass substrate with an average temperature of 85 °C. The polymerization front is formed a few seconds after deposition of the ink on the substrate and propagates along the as-deposited filament to transform the ink into a solid polymer (**Fig. 1a**). The experiment is monitored using an infrared (IR) camera to capture the temperature distribution of the material during the printing process (**Fig. 1b**). We neglect possible change of emissivity of DCPD during the curing process and a constant, calibrated emissivity of 0.9 is used for measuring the temperature distribution via infrared thermal imaging. The printing experiment in **Fig. 1b** is carried out using a pressure of 40 kPa and a printing velocity of 1.05 mm/s to 3D print a specimen consisting of four layers with a layer length of 20 mm. The printing velocity can be changed by changing the velocity of the nozzle and pressure used for dispensing. The printing velocity and layer length are two independent process parameters to study in this work.

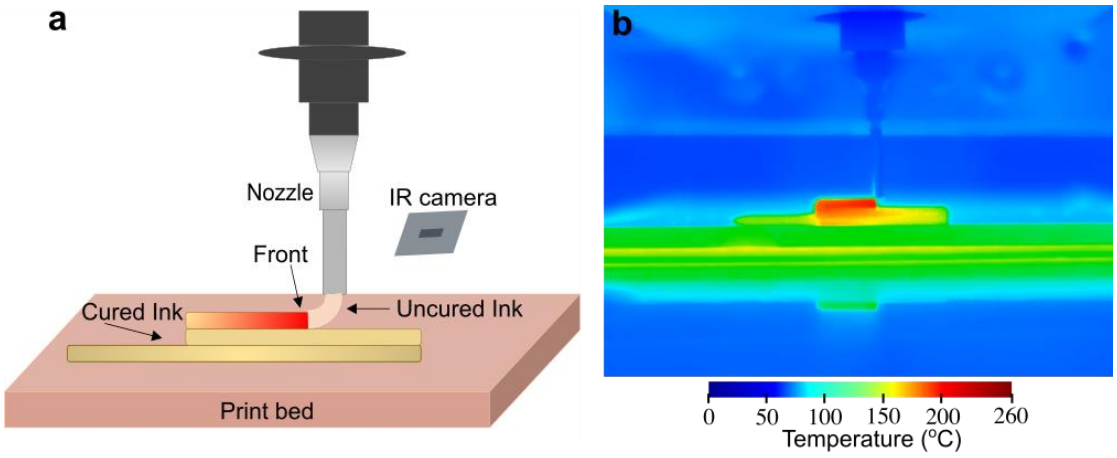

Fig. 1. (a) Schematic representation of the experimental setup. (b) Thermal image of the printing process captured by an IR camera.

2.2 Thermo-chemical modeling of the printing process

2.2.1 Reaction-diffusion model

In the AM process, we consider the thermal conduction and chemical reaction process associated with FP, which can be mathematically described by a coupled reaction-diffusion model that solves for the temperature field, T, and the degree-of-cure field, α (nondimensional), over space and time [22,23,33]:

$$\begin{cases} \nabla \cdot (\kappa \nabla T) + \rho H_{\mathrm{r}} \dfrac{\partial \alpha}{\partial t} = \rho C_{\mathrm{p}} \dfrac{\partial T}{\partial t} \\ \dfrac{\partial \alpha}{\partial t} = A exp(-\dfrac{E}{RT})(1-\alpha)^n \alpha^m \dfrac{1}{1+\exp\left(C(\alpha-\alpha_{\mathrm{c}}-\alpha_0)\right)} \end{cases}, \quad (1)$$

where the first equation is a diffusion equation with a source term characterized by the enthalpy of the reaction H_r (in J/kg). This term represents the heat generation from the chemical reaction and connects to the cure kinetics in the second equation through the curing rate. κ (in W/(m K)), ρ (in kg/m^3) and C_{p} (in J/(kg K)) respectively denote the thermal conductivity, density, and heat capacity of the printing ink. A (in 1/s) is the time constant; E (in J/mol) is the activation energy; R (8.314 J/(mol K)) is the universal gas constant; n and m are the two exponents that define the order of the reaction in the Prout-Tompkins model. C and α_{c} are two nondimensional constants introduced to include the effects of diffusion, and α_0 is the initial degree of cure. This model has been used for modeling of FP in neat resin and composite systems [23-26,33] and will be adopted to simulate the FP in the 3D printing process.

The initial degree of cure as well as cure kinetics are determined by performing differential scanning calorimetry (DSC) experiments on the ink using a modulated DSC (DSC 2500, TA Instrument). For DSC analysis, about 2-3 mg of uncured resin solution and pre-cured resin (ink) were transferred to hermetically sealed aluminum pans and heated from - 50 °C to 250 °C at a heating rate of 10 °C/min. The enthalpy of reaction

for each sample was determined by integrating the heat flow with respect to time after baseline correction (**Fig. 2a**). The initial degree of cure of the ink α_0 is calculated as

$$\alpha_0 = 1 - \frac{H_r}{H_t}, \tag{2}$$

where H_r and H_t refer to the enthalpy of reaction for ink and the neat resin, respectively. The initial degree of cure of the ink used in this work is 0.125. The DSC data of the ink and neat resin are shown in **Fig. 2a**, which can be transformed to the cure rate as a function of temperature in **Fig. 2b**. A constrained nonlinear multi-variable optimization algorithm [34] is adopted to determine the cure kinetics parameters that best fit the measured cure rate of the ink from the DSC measurements as shown in **Fig. 2b**. The fitted cure kinetic parameters are then adopted for 1D FP simulation to extract the front velocity. If the front velocity matches that of a test tube experiment, the fitted parameter are accepted; otherwise, this process is repeated until both the DSC fit and front velocity comparison are satisfactory. **Table 1** and **Table 2** summarize the fitted cure kinetic parameters, together with the thermal properties of DCPD from prior studies [35,36]. In the other regions of the simulation domain, such as the glass substrate and air surrounding the printing domain to be discussed next, only a heat conduction problem (i.e., the first equation of **Eq. (1)** without the source term) is solved for temperature, the physical and thermal properties of glass substrate and air are provided in **Table 2**.

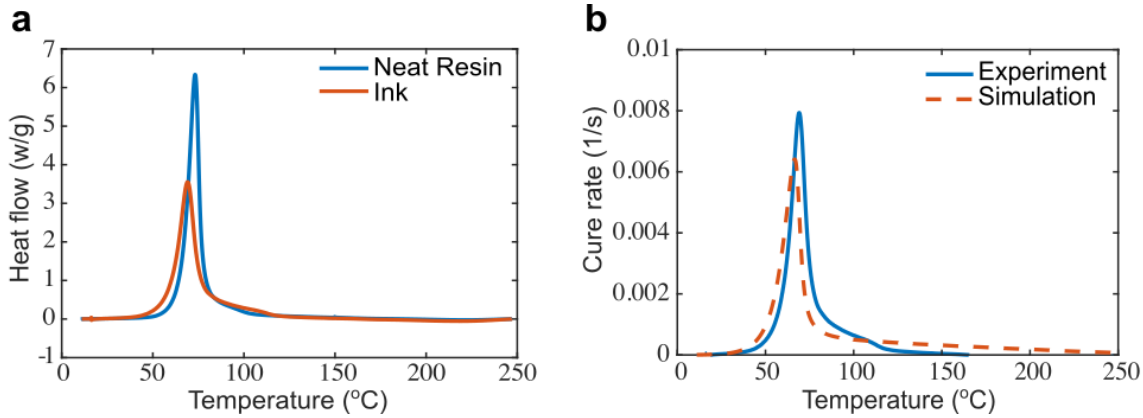

Fig. 2. (a) The heat flow as a function of temperature of the ink and neat resin from DSC measurements. (b) The fitted cure rate as a function of temperature.

Table 1

Cure kinetics parameters of the Prout-Tompkins model **Eq. (1)** for DCPD.

$A\ (\frac{1}{s})$	$E\ (\frac{J}{mol})$	n	m	α_c	C
3.13×10^{14}	103.54	1.68	0.83	0.58	28.12

Table 2
Thermal and physical properties of DCPD, glass substrate and air.

	$\kappa\ (\frac{W}{m\cdot k})$	$C_p\ (\frac{J}{kg\cdot k})$	$\rho\ (\frac{kg}{m^3})$	$H_r\ (\frac{J}{g})$
DCPD	0.15	1,600	980	340
Glass substrate	1.14	830	2,230	-
Air	0.03	1,003	1.2041	-

2.2.2 Model implementation

The coupled thermo-chemical model in **Eq. (1)** is solved using Multiphysics Object-Oriented Simulation Environment (MOOSE) [37]. MOOSE is an open source C++ finite element solver that combines an implicit Euler time stepping scheme and the pre-conditioned Jacobian-free Newton−Krylov scheme to solve the nonlinear system of equations at each time step [38,39]. Element activation is used to accomplish the ink deposition by continuously activating the subdomain into ink elements in the simulation domain following the prescribed printing path and velocity, over which **Eq. (1)** is solved to obtain the solution of temperature and degree of cure.

When simulating the 3D printing process, a printing path is first defined and an initial setup of the model is constructed as shown in **Fig. 3a**. This initial setup contains the mesh of the substrate, a small block of the ink representing the first drop of ink deposited on the print bed, and an air domain (gray region in **Fig. 3a**) encompassing the print bed and ink. This air domain overlaps with the printing path and will be changed to ink following the nozzle motion through element activation. It should be noted that the experimental 3D printing process starts by printing a straight filament

and the nozzle pauses temporarily at the start of the actual printing path for the front to initialize. When the front stabilizes and approaches the nozzle, the nozzle resumes its motion, where the actual printing starts and continues until the entire component is printed completely. The models use this printing path, but the printing velocity and layer length can vary.

To account for the effect of boundary conditions (i.e., heat loss from the ink to the environment), one could apply a convection to the outer boundary of the ink and update that boundary correspondingly as new ink is deposited. Alternatively, since the air temperature surrounding the ink is changing during the printing process, we consider an additional air domain (dark gray region in **Fig. 3a**), in which the heat loss to the air is accounted for through heat conduction. The glass substrate is also included in the simulation domain. As noted earlier, only the heat conduction problem is solved for temperature in the air (i.e., the entire light gray region as well as part of the dark gray region that has not yet been activated to be ink) and the substrate domain.

At the beginning of each time step, the simulation domain is first updated by changing some air elements in the gray region along the printing path into ink elements, the degree of cure and temperature of the new ink are initialized accordingly. Subsequently, the simulation domain is fixed in this time step to solve the temperature and degree of cure over the ink domain, and temperature over the substrate and air domain. Once the simulation of the current time step is finished, the above procedure is repeated for the next increment until the printing process is complete. A typical temperature contour of the printing domain is shown in **Fig. 3b**.

The initial simulation set up is the same as the experiment in **Fig. 1** for proper validation. Initial temperatures of the ink and substrate are 20 and 85 °C, respectively. The length of this filament for front initiation is 15 mm and the length of the actual printing area is 20 mm. The nozzle diameter is 1.6 mm, moving at a constant speed of 1.05 mm/s. The thickness of the glass substrate is 3.3 mm. A uniform element size of 0.05 mm × 0.05 mm is used to balance the accuracy and efficiency. The entire domain contains 226000

quadrilateral elements with 227227 nodes. **Fig. 3c-f** show simulated snap shots of temperature field associated with a four-layer printing process when printing each layer. Corresponding thermal images from experiments are shown in **Fig. 3g-j**. When printing the first layer as shown in **Fig. 3c**, **g**, a short filament is first printed, and the nozzle is paused temporarily before entering the actual printing path to initiate the reaction front and ensure the front is stable. The simulations well capture the high temperature of the front and the cold ink ahead of the reaction front. This comparison validates our model qualitatively and the model will be further validated and exercised to analyze the printing process in the following section.

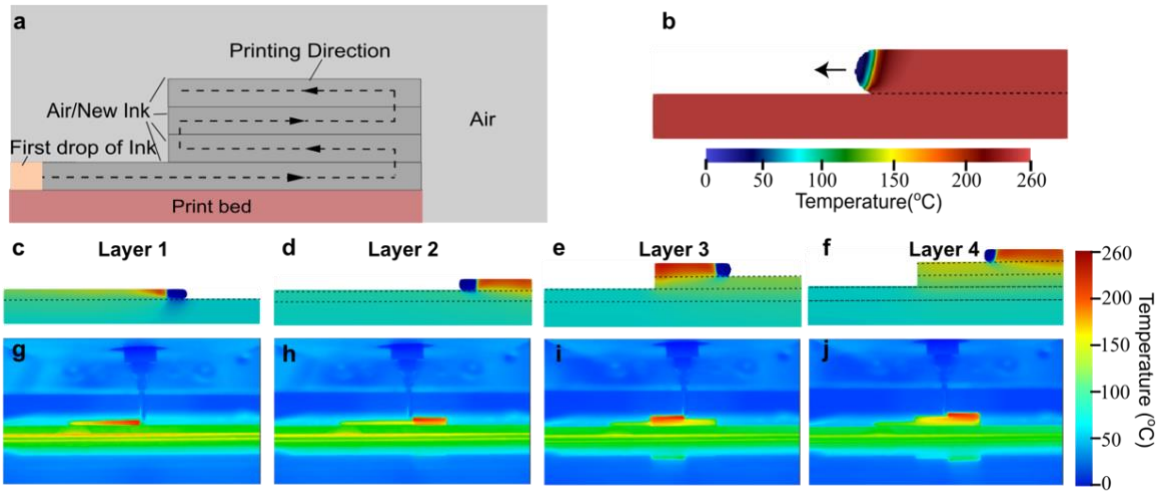

Fig. 3. (a) A schematic of the printing path and initial model setup. (b) A typical temperature contour during a printing process from simulation; Temperature snapshots of the 4-layer printing process from, simulations (c-f), and experiments (g-j) when nozzle reaches the middle of each layer.

3. Results and discussion

The focus of this work is to understand how the temperature and polymerization fields vary from different printing settings during the layer-by-layer FP-assisted 3D printing process and to explore the possibility to overcome certain challenges during the printing. This section will first quantitatively validate our model by comparing the simulated maximum temperature history during the printing process with the measured

experimental values, followed by a systematic study of the effect of various processing parameters. As there is a large number of processing parameters in the printing process, this study focuses on the printing velocity and the layer length, while the substrate temperature, the ambient temperature, and the ink composition remain the same as in the previous section. The heated print bed is the substrate for the first layer, then the previous layer will become the substrate for the current layer. In this paper, we focus on examining the effect of the above printing parameters on the front behavior, the distance between nozzle and front, the front and substrate temperatures, and the degree of cure of the printed components. The domain of model and definition of examined values are shown in **Fig. 4**.

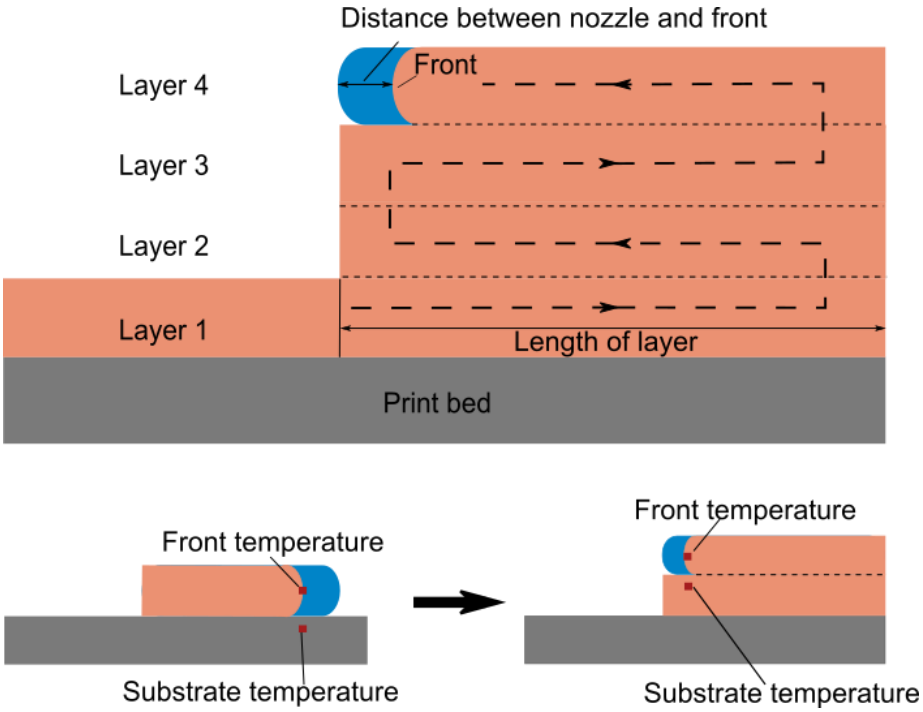

Fig. 4. Schematic of simulation domain and corresponding front and substrate temperature definition.

3.1 Model validation

In previous section, the temperature fields of the entire printing domain from experiments and simulations are qualitatively compared. To quantitatively validate the model, corresponding temperature distributions along the horizontal center line of the current layer in **Fig. 3c-f** (i.e., simulations) and g-j (i.e., experiments) are provided in

Fig 5a-d. Since the IR temperature measurement captures an average temperature over the pixel size of 0.181 mm × 0.181 mm (i.e., resolution of the IR camera), the simulated temperature field at the nodes of the finite element (FE) mesh in **Fig. 5e** is also averaged over an area equals to the size of the IR image pixel along the horizontal center line of the filament. Maximum temperature normally indicates the location of the reaction front, as shown and magnified in **Fig. 5e**. From the reaction front, a sharp drop is seen to the uncured side since uncured ink is cold, and a steady decrease is observed to the cured side due to cooling of the cured filament. The spatial temperature distribution in different layers and at different times in this 4-layer printing process are captured reasonably well in the simulations.

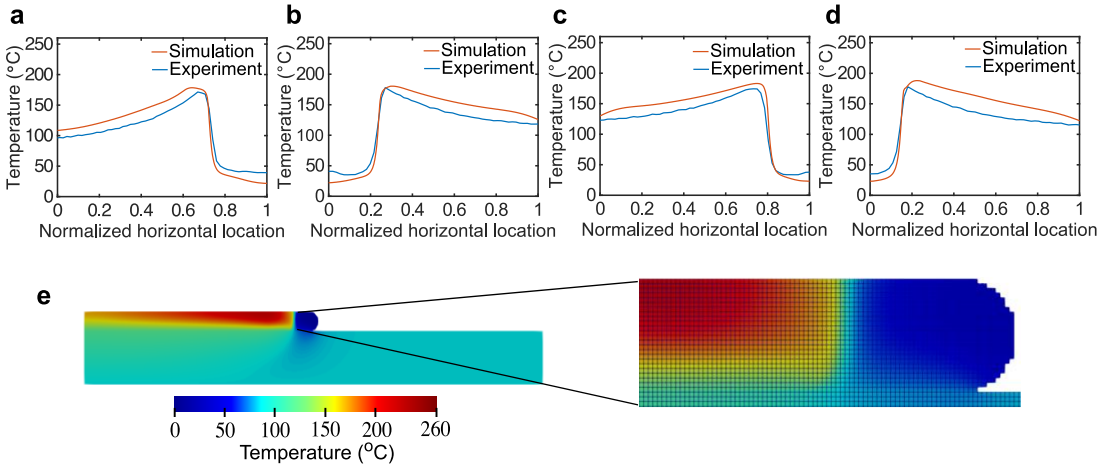

Fig. 5. (a-d) Temperature distribution along the horizontal center of the current layer at the same time points as in **Fig. 3**. (e) Temperature contour of the simulation and enlarged view of region around the front.

In addition to the spatial temperature distribution over a filament, we are interested in examining the temporal evolution of the front temperature during the printing process. The closest representation of front temperature is the maximum temperature in the current layer (e.g., see **Fig. 5a-d**). We therefore compare the front temperature evolution by extracting the maximum temperature of the current layer from both experiment and simulation over time in **Fig. 6**. Both the simulation and experiment show a relatively constant temperature fluctuations periodically when printing each

layer. At the end of each layer, when the nozzle is turning around to the next layer and the reaction front is also following the nozzle to the next layer, a temperature spike appears since the front temperature in the bottom region of the layer is higher than the substrate temperature, which initiates an even higher front temperature in the upper region of the layer, then the heat concentrated at the boundary between the ink and the air. Temperature spikes associated with reaction front hitting an insulative boundary (or less conductive material interface) have been previously observed [33]. After the turning process of each layer, the maximum temperature drops back to nearly constant with small fluctuations.

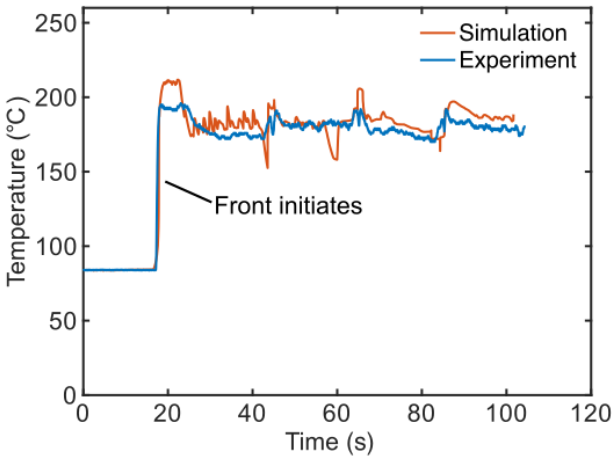

Fig. 6. Comparison of maximum temperature in the printing domain between simulation and experiment.

The simulation captures the overall trend reasonably well, however the temperature spike at the turning point is slightly larger than that measured by the IR camera. Possible reason for this discrepancy is because that IR camera only captures surface temperature, which may be lower than internal temperature of the ink filament. The current 2D simulation represents the middle plane of the filament between the front and back and captures the internal temperature of the filament.

3.2 Effect of printing velocity on the printing process

Recently, FP-assisted freeform 3D printing by Aw. [30] et al. showed that there is a narrow range of printing velocities that lead to a self-regulating behavior of the front to

either catch up with the nozzle or slow down to match the printing velocity. We use the validated model to study how the printing velocity is affecting the front behavior in the current layer-by-layer printing process.

Fig. 7a-d show the distribution of the degree of cure at the time when nozzle arrives at the end of the first layer at four different printing velocities: 0.8, 1.05, 1.5, and 1.8 mm/s. With the printing velocity ranging from 0.8 mm/s to 1.8 mm/s, the distance between the reaction front and the nozzle increases accordingly. The original simulation corresponded to the 3D printing experiment uses a printing velocity of 1.05 mm/s and yields good quality parts. Compared to this simulation, the 0.8 mm/s case has a very close distance between the front and the nozzle (i.e., 1.26 mm), while in the 1.5 and 1.8 mm/s cases, front falls further behind the nozzle, causing a long section of the extruded filament remaining in a temporarily uncured state before the arrival of the front. **Fig. 7e** shows the degree-of-cure distribution when nozzle arrives at the end of the second layer with a printing velocity of 1.8 mm/s, indicating an increased gap between the nozzle and front compared to that at the end of the first layer. When the printing continues to the third layer, the ink will be deposited on the uncured ink in the second layer. The presence of a gap between the solidified material and uncured ink usually leads to ink deformation and is accompanied with stress concentration [40-42]. If the distance between the reaction front and nozzle is too long, it can cause inaccurate printing due to possible deformation of the soft ink before being cured by the traveling front. This is especially important during the turning point of each layer. While our current model does not account for the mechanical deformation, an empirical maximum distance between the nozzle and front of 7 mm is considered based on multiple experiments. Thus, as long as the distance is within this limit, higher printing velocities can ensure faster printing.

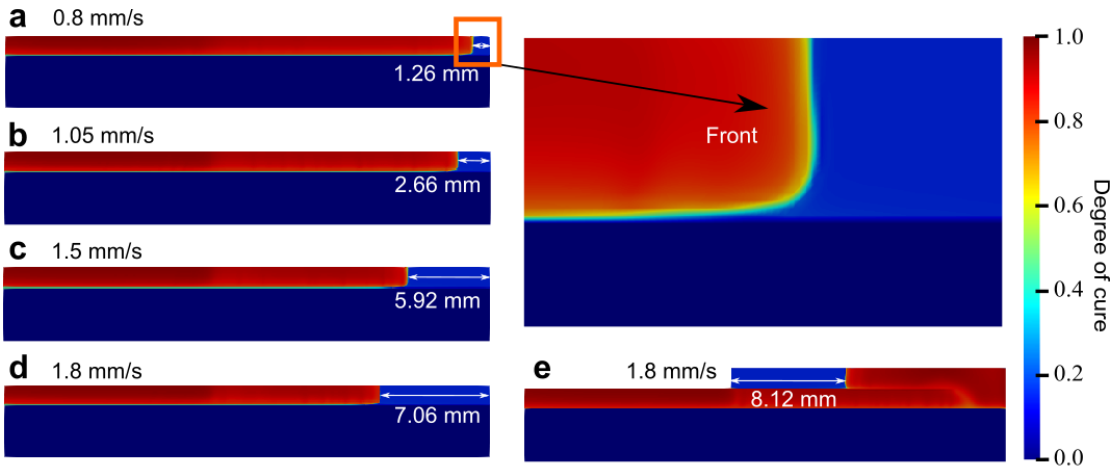

Fig. 7. (a-d) Degree of cure contours at the time when printing of the first layer is finished with different printing velocities. (e) Degree of cure contour when printing of the second layer is finished with a printing velocity of 1.8 mm/s.

The impact of the printing velocities on the front behavior is not limited to the first layer but can affect each layer through the entire printing process. For a single layer structure, the heated print bed provides heat for FP, but for this multi-layer structure, the heating source of each layer is the previously cured layer and varies from layer to layer. **Fig. 8a** shows the front temperature and substrate temperature for each layer at the time when printing of each layer is finished. The front temperature is extracted by finding the first point along the horizontal center line of each layer where the degree of cure reaches 0.5, while the substrate temperature is at the same vertical location below the layer, at 75% height of the layer thickness (as defined in **Fig. 4**). For a given printing velocity, we observed an increase in the substrate temperature over layers. The higher substrate temperature will lead to a higher front temperature in the current layer, which becomes the substrate temperature of the next layer. This cascading between substrate and reaction front leads to an increase in the substrate and front temperatures as the printing continues over layers. The only exception is the front temperature of the first layer, which is due to the higher heat conduction coefficient of the heating glass substrate than the printed polymer layers. When increasing the printing velocity, we also observed an increase in the substrate and front temperatures, which is mainly because the substrate layer has been cooled for a shorter period of time and lost less amount of heat at higher

printing velocities. A consequence of higher front temperature is higher front velocity, which leads to the change in the distance between the polymerization front and nozzle with respect to layer number and printing velocity as shown in **Fig. 8b**.

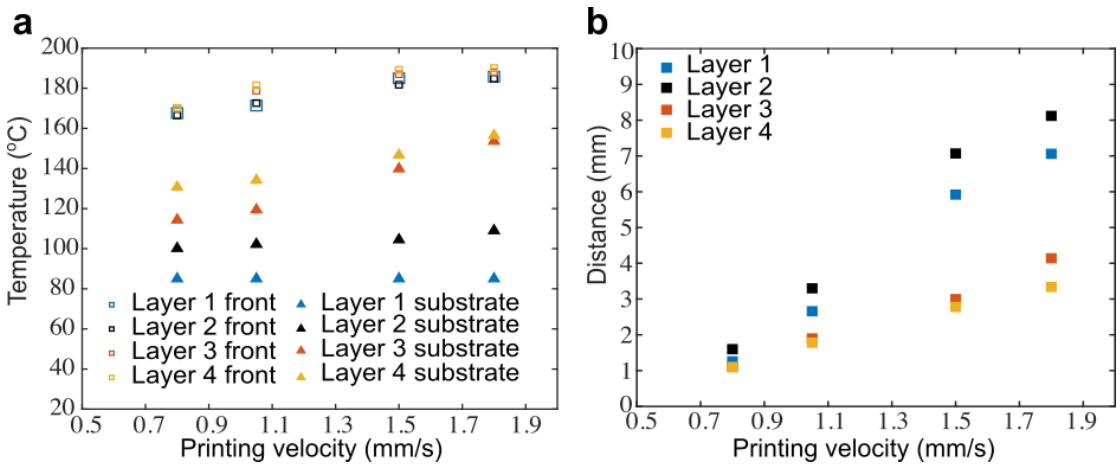

Fig. 8. (a) Front and substrate temperatures and (b) Distance between front and nozzle at the end of printing of each layer of various printing velocities.

In order to further analyze the impact of printing velocity on the degree of cure, we process the degree of cure at different times for different printing velocities. **Fig. 9a, b** depict the degree of cure along the horizontal center line of the first layer at the end of printing the second and the third layer, respectively, where the locations are normalized by the layer length. The degree of cure overall shows a constant value above 0.9 in most of the positions except the turning regions. At the turning region to the next layer, we first see a decrease in the degree of cure below 0.9 and then a ramp-up to a higher value than the overall degree of cure. The decrease in the degree of cure is because heat is absorbed by the cold ink in the next layer. The polymerization front meets the cold ink in the next layer earlier in the higher printing speed case (e.g., the distance between front and nozzle increases over layers as shown in **Fig. 8b**), hence the starting point of the decrease is earlier. The subsequent increase in the degree of cure is because of higher front temperatures (e.g., temperature spikes in **Fig. 6**) when the traveling front hits the boundary at the end of the layer. Among various printing velocities when the nozzle arrives at the end of the second layer, the instantaneous degree of cure is higher in faster printing cases. Similar observation can be made when the nozzle arrives at the

end of the third layer, with the only difference that the lower degree of cure close to the turning point now gets higher and close to the overall degree of cure. This indicates that the high temperature of the cured material after printing is further assisting the polymerization of those regions.

Since the cooling time of each layer varies during the printing process, when the fourth layer is printed, the cured material will still be in a cooling stage for some time. After the printed structure is cooled for 60 s, the temperature of the material in the first layer is around 110 °C and the degree of cure will not change anymore. The degree of cure along the center line of the printed part in the vertical direction for the slowest and fastest printing cases 60 s after the printing are plotted in **Fig. 9c**. The degree of cure shows an overall increasing trend over the layers, while periodically increasing from the bottom to the top of each layer, with a noticeable drop between layers. As we explained earlier, the front temperature is much higher at an insulative boundary (e.g., the boundary at the top surface of each layer), leading to higher degree of cure in the top region of each layer. In addition, the high front temperature of the next layer reheats and helps cure the top region of the previous layer, which further contributes to the gradient within each layer. Layer 4 is the last layer, which does not have this reheating effect, hence the increase of degree of cure is not as significant as those in other layers. Both effects do not exist at the bottom of each layer, leading the drop in degree of cure between layers. Based on **Fig. 8a**, the front temperatures show an overall increasing trend as layer number and printing velocity increase, which explains the overall increase of degree of from the bottom to the top of the part over layers, as well as the increase of printing velocity from 0.8 to 1.8 mm/s. Given the noticeable increase of degree of cure from 0.8mm/s to 1.8mm/s, it suggests that faster printing not only improves the efficiency but also the final degree of cure of the printed material.

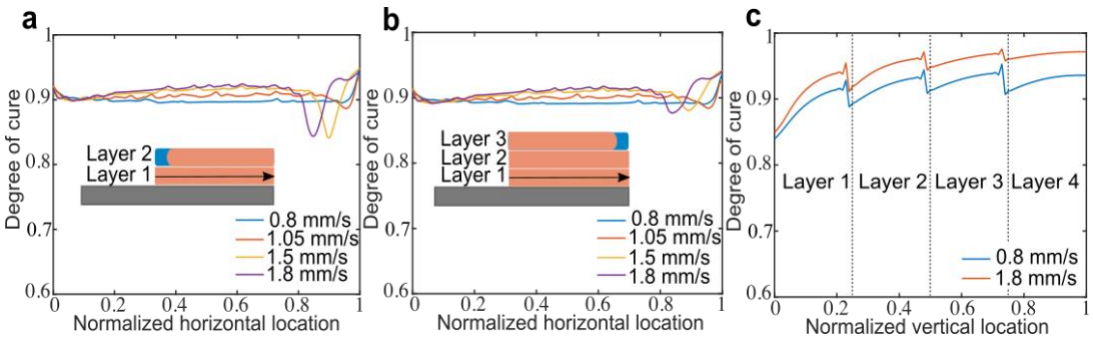

Fig. 9. Degree of cure along the center line of the first layer in the horizontal direction at the end of printing (a) the second layer and (b) the third layer for various printing velocities. (c) Degree of cure along center line through layers in the vertical direction 60 s after the printing completion for two different printing velocities.

Based on the previous study on the distance between the front and nozzle at different layers and printing velocities as well as the empirical information on the maximum distance (7 mm), it can be concluded that the 1.5 mm/s is the highest printing velocity should be used for the current ink to achieve a high printing efficiency, while ensuring the printing accuracy in the current setting for other printing parameters (e.g., ink and ambient temperature, nozzle diameter and ink composition). However, in practice, high productivity is always a goal for manufacturing; therefore, if the printer is equipped with a more advanced motion and dispensing control system, we can achieve even higher printing efficiency by designing a variable printing speed. For instance, one can design a printing process to slow down the nozzle speed during transition period between layers while keeping the velocity at a constant and high level in other regions, or set a pausing time at the turning of each layer to provide adequate time for front to catch up. When using a variable printing speed design, our model can be used to determine the optimal printing velocity history. When considering the degree of cure distribution within the printed structure, we need to account for the lower degree of cure of the first layer as well as the variations in the degree of cure around the turning region of each layer.

3.3 Effect of layer length on the printing process at constant printing velocity

From the previous study on the impact of printing velocity on the printing behavior, it is obvious that different printing velocities eventually lead to different front and substrate temperature of the ink at the onset of curing. Another factor that could potentially affect the ink and substrate temperature is the layer length which will be studied in this section.

The original simulation prints a four-layer structure with a length of 20 mm of each layer at the print velocity of 1.05 mm/s. **Fig. 10** shows the evolution of the degree of cure during the transition when nozzle is going from the second layer to the third layer. The reaction front follows nozzle path closely as the nozzle moves to the next layer. The distance between the front and nozzle at the end of printing of the first layer is 2.66 mm and no more than 3.5 mm throughout the entire printing process as shown in **Fig. 8b**.

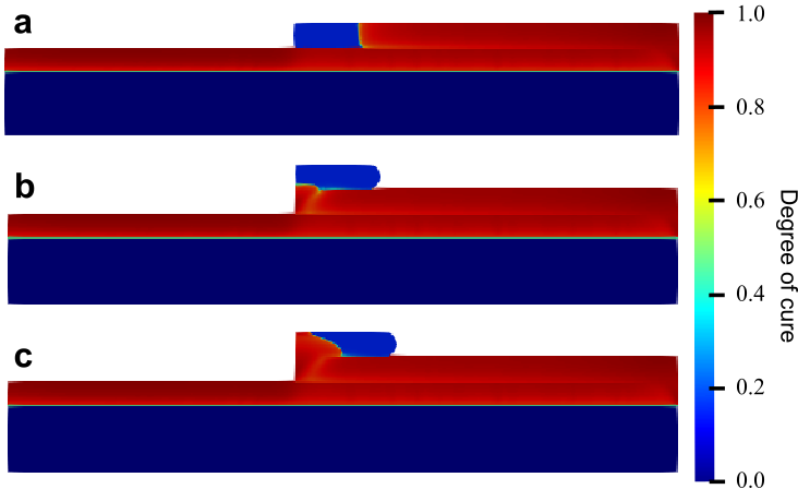

Fig. 10. Degree of cure contour of 20 mm printing length during the turning period between the second and the third layer.

Fig. 11 shows dissimilar front behaviors when the layer length is increased while all other parameters are kept the same. Specifically, when the printing is transitioning from the second layer to the third layer for the layer length of 40 and 60 mm, the front directly propagates to the next layer through the thickness direction which is perpendicular to the printing path, rather than along the printing path. Before the original front cures the

remaining of the previous layer, this generated front in the next layer will propagate back to cure the uncured portion of the ink in the previous and current layer.

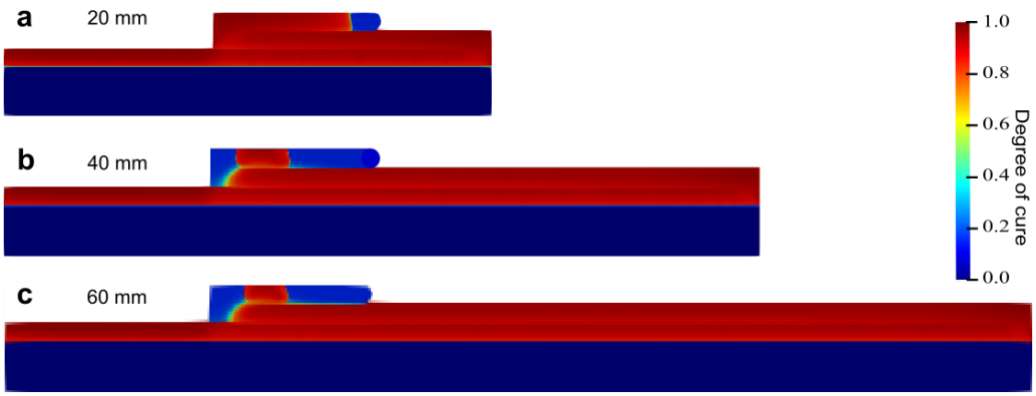

Fig. 11. Degree of cure contour at the time when nozzle is 12 mm away from the left side with layer length equal to (a) 20 mm, (b) 40 mm and (c) 60 mm.

This different front behavior for different layer lengths indicates that proper printing path needs to be designed when printing large structures. Further analysis of the evolution of both the degree of cure and corresponding temperature for the case with a 60 mm printing length are shown in **Fig. 12**. Initially, the front temperature is still high as shown in **Fig. 12e**. When the nozzle moves to the next layer, the cold ink is presented at both the left and the top of the current front, which absorbs heat, leading to a cool down of the front in **Fig. 12f**, and consequently the left-propagating front now temporarily pauses. At this moment, the ink temperature on the left and top of the front are similar, so the reaction front directly propagates to the top and stops its propagation to the left as shown in **Fig. 12f**. As the front hits the top boundary of the next layer, it will propagate both to the right (following the nozzle) and to the left to cure the ink on the left as shown in **Fig. 12g-h**.

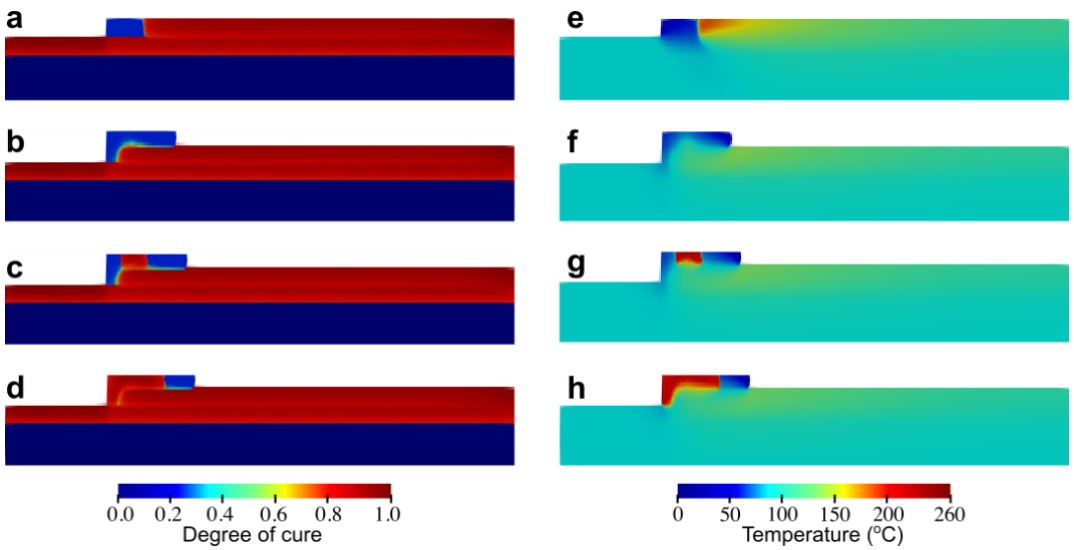

Fig. 12. (a-d) Degree of cure contour of 60 mm simulation. (e-h) Temperature contour of 60 mm simulation during the turning period between the second and the third layer.

Similar complications of front behavior are observed in other layers when printing a multi-layer structure. **Fig. 13** presents the distance between the front and nozzle for different printing lengths when the nozzle arrives the end of each layer. The distance increases monotonically as the layer length and layer number increases except for the first layer. For the first layer, the distance is around 2.8 mm for all three cases as the heated substrate has a relatively constant temperature (i.e., 85 °C), resulting in the same temperature and front speed for any points in the first layer. The minor effect of layer length on this layer indicates that the length is not a sensitive parameter when printing a single layer component. However, for other layers we observe a temperature gradient along the current substrate (i.e., previously printed layer), which in turn changes the front speed and temperature for the newly deposited layers and affects the distance between the front and the nozzle. In particular, when the printing length is 60 mm, a 5.5 mm gap is formed when the nozzle arrives at the end of the second layer. As previously described, a larger gap between the front and nozzle increases the risk of deformation; therefore, when printing large multi-layer structures, the layer dimension and printing path need to be carefully planned.

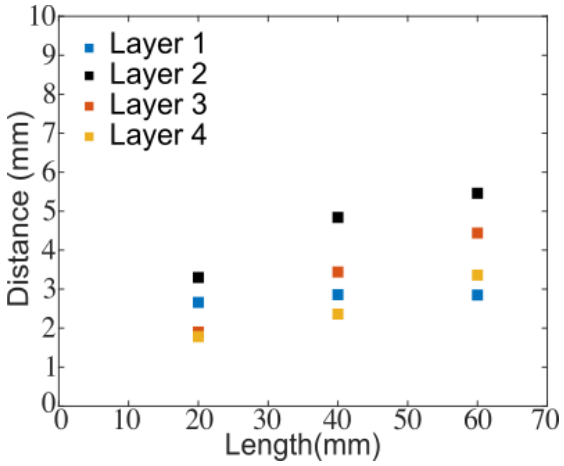

Fig. 13. Distance between front and nozzle at different layer lengths when printing of each layer is finished.

Temperature variation throughout layers is illustrated in **Fig. 14**. For each layer, the front and substrate temperature are extracted at ten equidistance time steps (normalized by the time for printing a single layer) and plotted in an increasing order from the start to the end of printing each layer. The front temperature and substrate temperature are defined in the previous section (**Fig. 4**). For the first layer, the relative stable temperature of all cases is consistent with what was observed in **Fig. 13** due to the stable temperature of the heated substrate. In other layers, both the front and substrate temperatures experience a decrease from the beginning to the end of each layer. This decrease in substrate temperature is because at the beginning of the current layer (i.e., layer 2, 3, and 4), the curing of the substrate is just finished and it does not cool down much, while toward the end of the current layer, the substrate has been cooled for a longer time. Additionally, as substrate provides heat to the ink, the front temperature directly follows the substrate temperature, which explains the trend of the front and substrate temperatures in **Fig. 14**. Overall, the substrate temperature is higher at higher layers, consistent with the analysis in Section 3.2. Moreover, as the printing length increases, the substrate temperature decreases due to a longer cool time before the ink is deposited on top of the substrate.

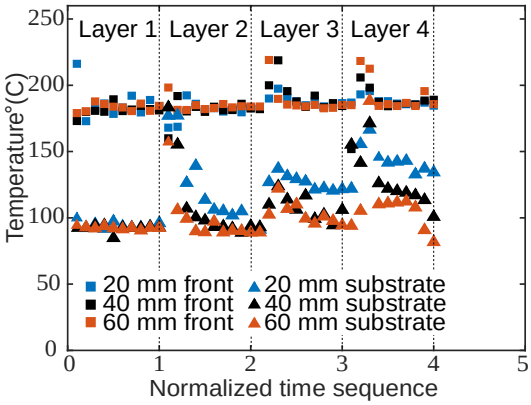

Fig. 14. Front temperature and corresponding substrate temperature of different layer lengths at the time when the nozzle reaches every one tenth of the layer length.

Increasing the layer length also affects the degree of cure in the printed structure. The degree of cure over the first layer at the end of printing of the second and the third layers are shown in **Fig. 15a, b**, respectively. The degree of cure of the first layer reaches over 0.9 and does not change much after the third layer is printed. In overall, even though the substrate temperature decreases when printing longer structure due to longer cooling times, the degree of cure still reaches 0.9 at most zones except at the end of the layer. The degree of cure through layers along the center line in the vertical direction 60 s after the entire structure is printed is plotted in **Fig. 15c**, degree of cure of both 20 and 60 mm cases increase with layer increases and are very close; however, due to the lower temperature in longer layer length in higher layers (**Fig. 14**), the degree of cure is slightly lower in the 60 mm case. The observation suggests that the layer length does not adversely affect the overall property of the printed structures.

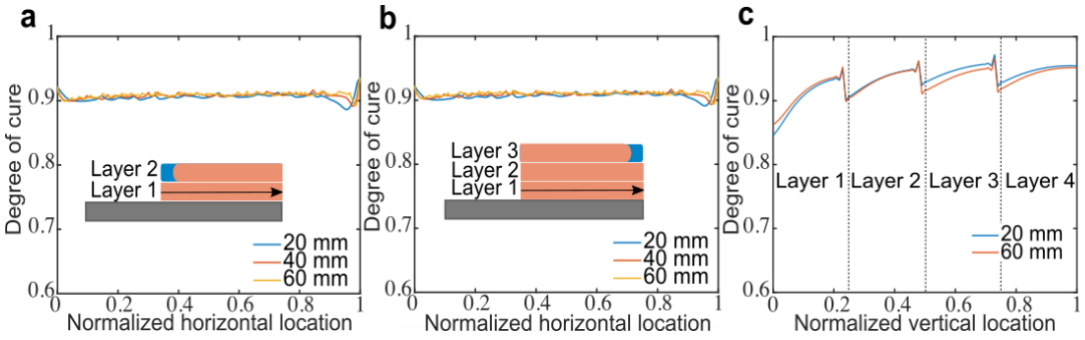

Fig. 15. Degree of cure along the center line of the first layer in the horizontal direction at the end of printing (a) the second layer and (b) the third layer for various layer lengths. (c) Degree of cure along center line through layers in the vertical direction 60 s after the printing is completed for two different layer lengths.

4. Conclusion

In this work, we have developed an experimentally validated thermo-chemical model to simulate the continuous layer-by-layer FP-assisted AM process for the first time. The continuous simulation enables us to capture the temperature evolution and provides insights regarding the degree of cure distribution and evolution during the printing process.

For the given ink composition, nozzle diameter and ambient temperature used in the current study, the printing velocity should be within a certain range (0.8-1.5 mm/s) such that the reaction front can follow the nozzle tightly (i.e., less than 7 mm based on empirical observations) to ensure printing accuracy. It is also observed that a higher printing velocity results in a higher degree of cure, which accelerates the production rate. Hence, the highest printing velocity should always be used while ensuring the distance between the nozzle and front is within the maximum allowed value (1.5 mm/s in the current study). To further improve printing efficiency, designing non-constant printing velocity that introduces pause time during the transition between layers could be considered. For printing a single layer structure, the layer length is not a vital parameter that needs to be considered but the effect of printing velocity cannot be ignored. When printing multi-layer structures, different layer lengths have a similar degree of cure, but a longer layer length has complications of front behavior at turning

regions. We also found that the front temperature plays an important role in the printing process and will be affected by the layer length and number of layers. The modeling results imply that the discrepency of front temperature and corresponding substrate temperature leads to variable front behaviors among different cases. This needs to be considered thoroughly when designing the printing path.

In summary, this is the first modeling of continuous layer-by-layer FP-assisted AM process. The simulation work in this paper enables the understanding of how different processing parameters are impacting the front behavior and temperature field during the printing process, and also provides guidance for the optimal design process. The modeling framework can also be adapted to simulate other printing processes that involve heat conduction and chemical reaction, such as photo-curing-based 3D printing process. Future work will focus on accounting for the flow and viscoelastic deformation of the ink and examining the interface bonding between different layers.

Acknowledgement

This work has been funded by the Wyoming NASA EPSCoR, NASA Grant #80NSSC19M0061. The research work carried out by M.Y. and M.Z. was supported by start-up funds from the Department of Mechanical Engineering at Colorado State University. M.Z. would like to acknowledge the summer internship award from the Energy Institute at Colorado State University. The computing resources and support at the Advanced Research Computing Center (ARCC) of University of Wyoming for the modeling work in this research is also greatly acknowledged.

Reference

[1]. A. Bîrcă, O. Gherasim, V. Grumezescu, and A.M. Grumezescu, *Introduction in thermoplastic and thermosetting polymers*, in *Materials for Biomedical Engineering*, Elsevier, 2019. pp. 1-28.

[2]. J.-P. Pascault, H. Sautereau, J. Verdu, and R.J. Williams, *Thermosetting polymers*, CRC press, Place, 2002.

[3]. M.A. Rahman, M.Z. Islam, L. Gibbon, C.A. Ulven, and J.J. La Scala, *3D printing of continuous carbon fiber reinforced thermoset composites using UV curable resin*, Polymer Composites. 42(2021) 5859-5868.

[4]. I.M. Daniel, O. Ishai, I.M. Daniel, and I. Daniel, *Engineering mechanics of composite materials*, Oxford university press New York, Place, 2006.

[5]. X. Xu, Y. Zhang, J. Jiang, H. Wang, X. Zhao, Q. Li, and W. Lu, *In-situ curing of glass fiber reinforced polymer composites via resistive heating of carbon nanotube films*, Composites Science and Technology. 149(2017) 20-27.

[6]. S. Agius, K. Magniez, and B. Fox, *Cure behaviour and void development within rapidly cured out-of-autoclave composites*, Composites Part B: Engineering. 47(2013) 230-237.

[7]. M. Herring,B. Fox, *The effect of a rapid curing process on the surface finish of a carbon fibre epoxy composite*, Composites Part B: Engineering. 42(2011) 1035-1043.

[8]. M.B.A. Tamez,I. Taha, *A review of additive manufacturing technologies and markets for thermosetting resins and their potential for carbon fiber integration*, Additive Manufacturing. 37(2021) 101748.

[9]. B. Shi, Y. Shang, P. Zhang, A.P. Cuadros, J. Qu, B. Sun, B. Gu, T.-W. Chou, and K.K. Fu, *Dynamic capillary-driven additive manufacturing of continuous carbon fiber composite*, Matter. 2(2020) 1594-1604.

[10]. O. Uitz, P. Koirala, M. Tehrani, and C.C. Seepersad, *Fast, low-energy additive manufacturing of isotropic parts via reactive extrusion*, Additive Manufacturing. 41(2021) 101919.

[11]. R.R. Fernandes, N. van de Werken, P. Koirala, T. Yap, A.Y. Tamijani, and M. Tehrani, *Experimental investigation of additively manufactured continuous fiber reinforced composite parts with optimized topology and fiber paths*, Additive Manufacturing. 44(2021) 102056.

[12]. M. Mahmoudi, S.R. Burlison, S. Moreno, and M. Minary-Jolandan, *Additive-Free and Support-Free 3D Printing of Thermosetting Polymers with Isotropic Mechanical Properties*, ACS Appl Mater Interfaces. 13(2021) 5529-5538.

[13]. D. Lei, Y. Yang, Z. Liu, S. Chen, B. Song, A. Shen, B. Yang, S. Li, Z. Yuan, and Q. Qi, *A general strategy of 3D printing thermosets for diverse applications*, Materials Horizons. 6(2019) 394-404.

[14]. M. Röttger, T. Domenech, R. van der Weegen, A. Breuillac, R. Nicolaÿ, and L. Leibler, *High-performance vitrimers from commodity thermoplastics through dioxaborolane metathesis*, Science. 356(2017) 62-65.

[15]. B. Wang, Z. Zhang, Z. Pei, J. Qiu, and S. Wang, *Current progress on the 3D printing of thermosets,* Advanced Composites and Hybrid Materials. 3(2020) 462-472.

[16]. M.G. Odom, C.B. Sweeney, D. Parviz, L.P. Sill, M.A. Saed, and M.J. Green, *Rapid curing and additive manufacturing of thermoset systems using scanning microwave heating of carbon nanotube/epoxy composites,* Carbon. 120(2017) 447-453.

[17]. N. Nawafleh,E. Celik, *Additive manufacturing of short fiber reinforced thermoset composites with unprecedented mechanical performance,* Additive Manufacturing. 33(2020) 101109.

[18]. I.D. Robertson, M. Yourdkhani, P.J. Centellas, J.E. Aw, D.G. Ivanoff, E. Goli, E.M. Lloyd, L.M. Dean, N.R. Sottos, and P.H. Geubelle, *Rapid energy-efficient manufacturing of polymers and composites via frontal polymerization,* Nature. 557(2018) 223-227.

[19]. J.A. Pojman, *Frontal Polymerization*, in *Polymer Science: A Comprehensive Reference*, 2012. pp. 957-980.

[20]. A.M. Khan,J.A. Pojman, *The use of frontal polymerization in polymer synthesis,* Trends in Polymer Science. 8(1996) 253-257.

[21]. M. Ziaee,M. Yourdkhani, *Effect of resin staging on frontal polymerization of dicyclopentadiene,* Journal of Polymer Science. 59(2021) 1732-1739.

[22]. S. Vyas, E. Goli, X. Zhang, and P. Geubelle, *Manufacturing of unidirectional glass-fiber-reinforced composites via frontal polymerization: A numerical study,* Composites Science and Technology. 184(2019) 107832.

[23]. S. Vyas, X. Zhang, E. Goli, and P. Geubelle, *Frontal vs. bulk polymerization of fiber-reinforced polymer-matrix composites,* Composites Science and Technology. 198(2020) 108303.

[24]. E. Goli, N.A. Parikh, S.K. Vyas, X. Zhang, N.R. Sottos, J.S. Moore, and P.H. Geubelle, *Manufacturing of carbon- And glass-fiber composites using frontal polymerization*, in *22nd International Conference on Composite Materials*. 2019: Melbourne.

[25]. M. Garg, J.E. Aw, X. Zhang, P.J. Centellas, L.M. Dean, E.M. Lloyd, I.D. Robertson, Y. Liu, M. Yourdkhani, and J.S. Moore, *Rapid synchronized fabrication of vascularized thermosets and composites,* Nature communications. 12(2021) 1-9.

[26]. P. Centellas, M. Garg, Z. Chen, X. Zhang, N. Parikh, P.H. Geubelle, and N.R. Sottos, *Energy-Efficient Manufacturing of Multifunctional Vascularized Composites,* Journal of composite materials. (2022).

[27]. A. Mariani, S. Fiori, Y. Chekanov, and J.A. Pojman, *Frontal ring-opening metathesis polymerization of dicyclopentadiene,* Macromolecules. 34(2001) 6539-6541.

[28]. Q. Li, H.-X. Shen, C. Liu, C.-f. Wang, L. Zhu, and S. Chen, *Advances in Frontal Polymerization Strategy: from Fundamentals to Applications,* Progress in Polymer Science. (2022) 101514.

[29]. I.D. Robertson, M. Yourdkhani, P.J. Centellas, J.E. Aw, D.G. Ivanoff, E. Goli, E.M. Lloyd, L.M. Dean, N.R. Sottos, P.H. Geubelle, J.S. Moore, and S.R. White, *Rapid energy-efficient manufacturing of polymers and composites via frontal polymerization,* Nature. 557(2018) 223-227.

[30]. J.E. Aw, X. Zhang, A.Z. Nelson, L.M. Dean, M. Yourdkhani, R.H. Ewoldt, P.H. Geubelle, and N.R. Sottos, *Self-regulative Direct Ink Writing of Frontally Polymerizing Thermoset Polymers,* Advanced Materials Technologies. (2022).

[31]. M. Ziaee,M. Yourdkhani, *3D Printing of Short Carbon Fiber Composites via Frontal Polymerization*.in *Proceedings of the American Society for Composites—Thirty-Sixth Technical Conference on Composite Materials*.2021.

[32]. M. Ziaee, J.W. Johnson, and M. Yourdkhani, *3D Printing of Short-Carbon-Fiber-Reinforced Thermoset Polymer Composites via Frontal Polymerization,* ACS Applied Materials & Interfaces. 14(2022) 16694-16702.

[33]. E. Goli, I.D. Robertson, P.H. Geubelle, and J.S. Moore, *Frontal Polymerization of Dicyclopentadiene: A Numerical Study,* J Phys Chem B. 122(2018) 4583-4591.

[34]. M.J.D. Powell, *Numerical Analysis*.in *Proceedings of the Biennial Conference*.1977.Dundee.

[35]. M. Garg, S.R. White, and N.R. Sottos, *Rapid degradation of poly (lactic acid) with organometallic catalysts,* ACS Applied Materials & Interfaces. 11(2019) 46226-46232.

[36]. M. Garg, A.C. Ladd, J.E. Aw, X. Zhang, and N.R. Sottos, *Sacrificial Cyclic Poly (phthalaldehyde) Templates for Low-Temperature Vascularization of Polymer Matrices,* ACS Applied Polymer Materials. (2021).

[37]. D. Gaston, C. Newman, G. Hansen, and D. Lebrun-Grandie, *MOOSE: A parallel computational framework for coupled systems of nonlinear equations*, Nuclear Engineering and Design. 239(2009) 1768-1778.

[38]. D.A. Knoll,D.E. Keyes, *Jacobian-free Newton–Krylov methods: a survey of approaches and applications*, Journal of Computational Physics. 193(2004) 357-397.

[39]. M. Pernice,H.F. Walker, *NITSOL: A Newton iterative solver for nonlinear systems*, SIAM Journal on Scientific Computing. 19(1998) 302-318.

[40]. X. Wang, M. Jiang, Z. Zhou, J. Gou, and D. Hui, *3D printing of polymer matrix composites: A review and prospective*, Composites Part B: Engineering. 110(2017) 442-458.

[41]. M. Namiki, M. Ueda, A. Todoroki, Y. Hirano, and R. Matsuzaki, *3D printing of continuous fiber reinforced plastic*.in *SAMPE Tech Seattle 2014 Conference*.2014. Soc. for the Advancement of Material and Process Engineering.

[42]. H.L. Tekinalp, V. Kunc, G.M. Velez-Garcia, C.E. Duty, L.J. Love, A.K. Naskar, C.A. Blue, and S. Ozcan, *Highly oriented carbon fiber–polymer composites via additive manufacturing*, Composites Science and Technology. 105(2014) 144-150.